Perturbation compensation-based non-linear adaptive control of ESS-DVR for the LVRT capability improvement of wind farms

Linfang Yan[1], Xia Chen[1] ✉, Xin Zhou[1,2], Haishun Sun[1], Lin Jiang[2]

[1]*State Key Laboratory of Advanced Electromagnetic Engineering and Technology, Huazhong University of Science and Technology, Wuhan, People's Republic of China*

[2]*Department of Electrical Engineering and Electronics, The University of Liverpool, Liverpool, UK*

✉ *E-mail: cxhust@hust.edu.cn*

Abstract: This study presents a non-linear adaptive control (NAC) for the energy storage system (ESS) embedded dynamic voltage restorer (DVR) in enhancing the low-voltage ride through (LVRT) capability of wind farms. The proposed NAC features a perturbation observer to estimate and then compensate the real perturbation of the whole system, including parameter uncertainties, measurement noise, and external disturbances such as different grid faults and intermittent wind power. It can achieve an adaptive and robust control without requiring accurate system model and full-state measurements. This control is then applied to the ESS embedded DVR (ESS-DVR) system, in which the ESS can store the blocked wind power for potential power fluctuation suppression. Simulation studies have verified that the proposed control for ESS-DVR can effectively enhance the LVRT capability of wind farms installed with different types of WTGs under different operating conditions. Moreover, its superiority has also been demonstrated by comparing with fixed gains-based conventional vector control and accurate system model-based feedback linearising control.

1 Introduction

The increasing penetration of wind power has forced power system operators to introduce new grid codes to accommodate more renewable generations [1]. Different from traditional generators, early wind turbine generators (WTGs) are generally not required to withstand low voltage due to their small capacities. Consequently, WTGs will be disconnected from the grid to protect themselves under voltage disturbances. However, large-scale wind farms, which consist of many WTGs connected together by overhead lines or cables, now have capacity comparable to that of conventional power generators. The disconnection of wind farms will cause a large amount of power shortage. Therefore, wind farms are expected to remain connected to the grid and even support the grid such as voltage restoration by providing reactive power during and after grid faults or disturbances. This is known as low-voltage ride through (LVRT) capability, which is required by most grid codes [2].

The LVRT capability of wind farms can be improved from two aspects, i.e. the WTG and the wind farm. Regarding the WTG, with the merit of without modifying the current hardware and additional cost, improving the control strategy of WTGs is an effective and economical way [3, 4], such as the modified pitch angle control proposed in [5] and the modified converter control presented in [6–8]. Another effective alternative approach is to modify the hardware of converters or install additional protection devices inside the WTG [2], such as energy storage system (ESS) [9], crowbar [10], DC-link chopper [11], and series dynamic resistor [12]. The reactive power compensation devices are generally required to directly support the voltage level at the point of common coupling (PCC) of wind farms [2], such as the static synchronous compensator (STATCOM) [13], static var compensator (SVC) [14], and dynamic voltage restorer (DVR) [15]. Furthermore, compared with the parallel-connected STATCOM and SVC, the series-connected DVR could be more effective because it can isolate the wind farm's PCC from the grid voltage disturbances and maintain an almost constant voltage level at the PCC, although the DVR increases the system complexity and cost. Hence, less requirements on the protection system of wind farms are needed. Owing to these advantages, DVR has been widely used to improve the LVRT capability of doubly fed induction generator (DFIG)-based wind farms [15–18] and the squirrel cage induction generator-based wind farm [19]. On the other hand, an ESS is generally embedded in the DC side of the DVR to store the blocked wind power and suppress potential wind power fluctuation.

Various control methods have been employed for DVR controller design, such as the conventional vector control (VC) in [15–21]. However, this control method is designed and tuned based on one operating point, easily resulting in weaken control performance under varying operation conditions. To improve the performance of the VC, advanced control methods such as fuzzy control [22, 23], H-inf control [24], neural network control [25], and feedback linearising control (FLC) [26–29] have been proposed. Some of those controllers, such as the FLC, require accurate system models and parameter values, which in turn result in a complex control law and weak robustness. Most importantly, wind farms are generally operated and are subject to varying operational conditions, model uncertainties, and external disturbances. Consequently, a robust DVR control strategy is essential for the field implementation.

This paper presents the perturbation compensation-based non-linear adaptive control (NAC) for the ESS-DVR to improve the LVRT capability of wind farms. The NAC method is one type of disturbance observers-based adaptive control, which have been applied to control the grid-side converter (GSC) and improve the LVRT capability of a permanent magnet synchronous generator (PMSG)-based WTG [30] and also in multi-machine power system stability [31–33]. Based on perturbation estimation and compensation, all coupling non-linear dynamics, uncertainties, and external disturbances, especially different grid voltage dips and the uncertain wind power input, can be fully compensated. Moreover, no accurate system model and full-state feedbacks are required, making the controller more realistic and easier to implement.

The remainder of this paper is organised as follows. Section 2 presents the modelling of a wind farm with an ESS-DVR. The perturbation compensation-based NAC is designed for the ESS-DVR in Section 3. Simulation results are presented in Section 4 and final conclusions are drawn in Section 5.

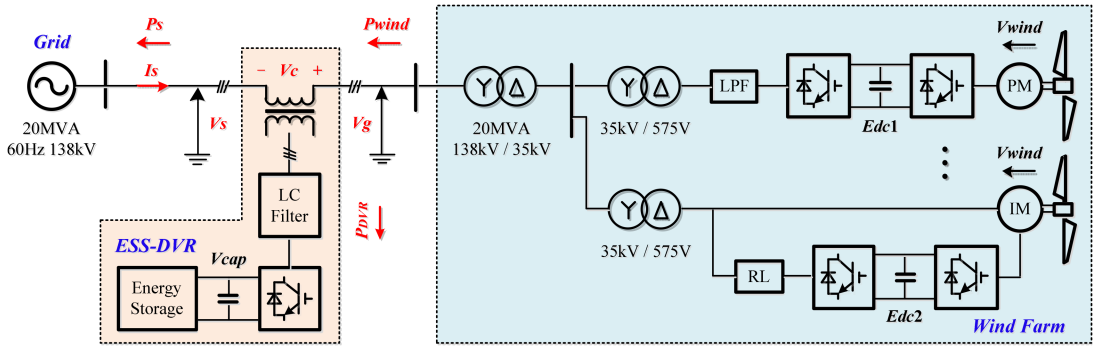

Fig. 1 *System configuration*

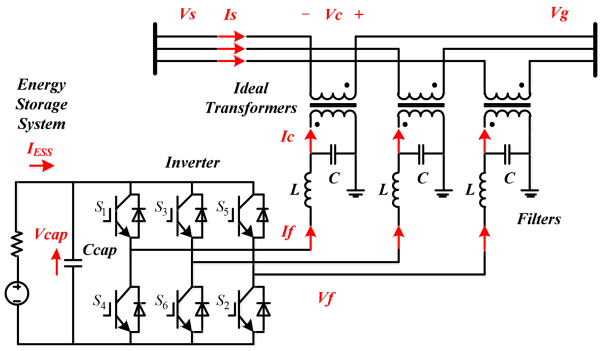

Fig. 2 *Structure of the ESS-DVR*

2 Modelling of the ESS-DVR

The configuration of the overall system is shown in Fig. 1. It comprises an ESS-DVR and a wind farm installed with a 10 MW PMSG-WTG and a 10 MW DFIG-WTG. The ESS-DVR is connected in series with the power line via three single-phase ideal transformers. The detailed electric circuit of ESS, inverter, filters, and ideal transformers in ESS-DVR is shown in Fig. 2.

The rating of the ESS-DVR mainly relies on the depth of the voltage fault that should be compensated [15]

$$S_{\mathrm{ESS-DVR}} = \left(\frac{V_{\mathrm{rated}} - V_{\mathrm{fault}}}{V_{\mathrm{rated}}}\right) \cdot S_{\mathrm{WF}} \tag{1}$$

where $S_{\mathrm{ESS\text{-}DVR}}$ is the ESS-DVR capacity (including ESS and inverter etc.), S_{WF} is the wind farm capacity, V_{rated} the rated grid voltage, and V_{fault} the depth of voltage fault.

As shown in Fig. 2, the mathematical model of the ESS-DVR is given by

$$\begin{cases} V_f = L \cdot \dfrac{\mathrm{d}I_f}{\mathrm{d}t} + V_{\mathrm{c}} \\ I_f = C \cdot \dfrac{\mathrm{d}V_{\mathrm{c}}}{\mathrm{d}t} + I_{\mathrm{c}} \\ I_{\mathrm{ESS}} = C_{\mathrm{cap}} \cdot \dfrac{\mathrm{d}V_{\mathrm{cap}}}{\mathrm{d}t} + \dfrac{\mathrm{Re}(V_{\mathrm{c}} \cdot I_{\mathrm{c}}^{*})}{V_{\mathrm{cap}}} \end{cases} \tag{2}$$

where C and L are the capacitance and inductance of filters, respectively. C_{cap} is the DC-link capacitor in ESS-DVR. V_{cap} is the DC-link voltage. I_{ESS} is the output current of ESS. V_s is the grid voltage. V_g is the wind farm voltage. V_f and I_f are the output voltage and current of the inverter, respectively. V_{c} is the compensation voltage. I_{c} is the compensation current and has the following relationship with the output current of the wind farm I_s

$$I_{\mathrm{c}} = I_s \tag{3}$$

Under the synchronously rotating d–q reference frame, the state-space model of the ESS-DVR can be obtained as (see (4)) . System outputs are defined as

$$\begin{bmatrix} y_1 \\ y_2 \end{bmatrix} = \begin{bmatrix} V_{\mathrm{c}\_d} \\ V_{\mathrm{c}\_q} \end{bmatrix} \tag{5}$$

where (V_{f_d}, V_{f_q}), (V_{c_d}, V_{c_q}), (I_{f_d}, I_{f_q}), and (I_{s_d}, I_{s_q}) are the d-axis and q-axis components of the three-phase voltage (V_f, V_{c}) and the three-phase current (I_f I_s), respectively.

3 Controller design of the ESS-DVR

3.1 Non-linear adaptive control

3.1.1 Input–output linearisation: Considering a multiple-input multiple output system

$$\begin{bmatrix} \dfrac{\mathrm{d}I_{f\_d}}{\mathrm{d}t} \\ \dfrac{\mathrm{d}I_{f\_q}}{\mathrm{d}t} \\ \dfrac{\mathrm{d}V_{\mathrm{c}\_d}}{\mathrm{d}t} \\ \dfrac{\mathrm{d}V_{\mathrm{c}\_q}}{\mathrm{d}t} \\ \dfrac{\mathrm{d}V_{\mathrm{cap}}}{\mathrm{d}t} \end{bmatrix} = \begin{bmatrix} \omega \cdot I_{f\_q} - \dfrac{1}{L} \cdot V_{\mathrm{c}\_d} \\ -\omega \cdot I_{f\_d} - \dfrac{1}{L} \cdot V_{\mathrm{c}\_q} \\ \omega \cdot V_{\mathrm{c}\_q} + \dfrac{1}{C} \cdot I_{f\_d} - \dfrac{1}{C} \cdot I_{s\_d} \\ -\omega \cdot V_{\mathrm{c}\_d} + \dfrac{1}{C} \cdot I_{f\_q} - \dfrac{1}{C} \cdot I_{s\_q} \\ -\dfrac{3}{2} \cdot \dfrac{V_{\mathrm{c}\_d} \cdot I_{s\_d} + V_{\mathrm{c}\_q} \cdot I_{s\_q}}{C_{\mathrm{cap}} \cdot V_{\mathrm{cap}}} + \dfrac{I_{\mathrm{ESS}}}{C_{\mathrm{cap}}} \end{bmatrix} + \begin{bmatrix} \dfrac{1}{L} & 0 \\ 0 & \dfrac{1}{L} \\ 0 & 0 \\ 0 & 0 \\ 0 & 0 \end{bmatrix} \begin{bmatrix} V_{f\_d} \\ V_{f\_q} \end{bmatrix} \tag{4}$$

$$\begin{cases} \dot{\boldsymbol{x}} = \boldsymbol{f}(\boldsymbol{x}) + \boldsymbol{g}(\boldsymbol{x}) \cdot \boldsymbol{u} \\ \boldsymbol{y} = \boldsymbol{h}(\boldsymbol{x}) \end{cases} \tag{6}$$

where $\boldsymbol{x} \in R^n$ is the state vector, $\boldsymbol{u} \in R^m$ the control input vector, $\boldsymbol{y} \in R^m$ the system output vector, and $\boldsymbol{f}(\boldsymbol{x})$, $\boldsymbol{g}(\boldsymbol{x})$, and $\boldsymbol{h}(\boldsymbol{x})$ are the smooth vector fields.

Input–output linearisation of the system can be written as:

$$\begin{bmatrix} y_1^{(r_1)} \\ \vdots \\ y_m^{(r_m)} \end{bmatrix} = \begin{bmatrix} L_f^{r_1} \cdot h_1 \\ \vdots \\ L_f^{r_m} \cdot h_m \end{bmatrix} + \boldsymbol{B}(x) \cdot \begin{bmatrix} u_1 \\ \vdots \\ u_m \end{bmatrix} \tag{7}$$

where $\boldsymbol{B}(x)$ is the control gain matrix. If $\boldsymbol{B}(x)$ is invertible, a new control input vector $\boldsymbol{v} \in R^m$ can be introduced

$$\begin{bmatrix} u_1 \\ \vdots \\ u_m \end{bmatrix} = \boldsymbol{B}^{-1}(x) \cdot \left\{ -\begin{bmatrix} L_f^{r_1} \cdot h_1 \\ \vdots \\ L_f^{r_m} \cdot h_m \end{bmatrix} + \begin{bmatrix} v_1 \\ \vdots \\ v_m \end{bmatrix} \right\} \tag{8}$$

Now, the new input–output relations are given by

$$\begin{bmatrix} y_1^{(r_1)} \\ \vdots \\ y_m^{(r_m)} \end{bmatrix} = \begin{bmatrix} v_1 \\ \vdots \\ v_m \end{bmatrix} \tag{9}$$

Thus, the desired dynamics can be imposed on the system output $\boldsymbol{y}$ by the new control input $\boldsymbol{v}$.

3.1.2 Perturbation observer: Assume that all non-linearities of the system (7) are unknown, and thus define perturbation terms as

$$\begin{bmatrix} \Psi_1 \\ \vdots \\ \Psi_m \end{bmatrix} = \begin{bmatrix} L_f^{r_1} \cdot h_1 \\ \vdots \\ L_f^{r_m} \cdot h_m \end{bmatrix} + [\boldsymbol{B}(x) - \boldsymbol{B}_0] \cdot \begin{bmatrix} u_1 \\ \vdots \\ u_m \end{bmatrix} \tag{10}$$

where Ψ_i, $i = 1, \ldots, m$, is the perturbation term, and $\boldsymbol{B}_0$ the nominal control gain matrix. Then, the system (7) can be rewritten as

$$\begin{bmatrix} y_1^{(r_1)} \\ \vdots \\ y_m^{(r_m)} \end{bmatrix} = \begin{bmatrix} \Psi_1 \\ \vdots \\ \Psi_m \end{bmatrix} + \boldsymbol{B}_0 \cdot \begin{bmatrix} u_1 \\ \vdots \\ u_m \end{bmatrix} \tag{11}$$

For the ith subsystem, by defining state variables as: $w_{i,1} = y_i, \ldots, w_{i,r_i} = y_i^{(r_i-1)}$, and a virtual state variable to denote the perturbation $w_{i,r_i+1} = \Psi_i$, the ith subsystem can be represented as

$$\begin{cases} \dot{w}_{i,1} = w_{i,2} \\ \vdots \\ \dot{w}_{i,r_i} = w_{i,r_i+1} + \boldsymbol{B}_{0i} \cdot \boldsymbol{u} \\ \dot{w}_{i,r_i+1} = \dot{\Psi}_i \end{cases} \tag{12}$$

where $\boldsymbol{B}_{0i}$ is the ith row of the $\boldsymbol{B}_0$. For the subsystem (12), a high gain observer [30] is proposed to estimate the states and the perturbation as

$$\begin{cases} \dot{\hat{w}}_{i,1} = \hat{w}_{i,2} + l_{i,1} \cdot (w_{i,1} - \hat{w}_{i,1}) \\ \vdots \\ \dot{\hat{w}}_{i,r_i} = \hat{w}_{i,r_i+1} + l_{i,r_i} \cdot (w_{i,1} - \hat{w}_{i,1}) + \boldsymbol{B}_{0i} \cdot \boldsymbol{u} \\ \dot{\hat{w}}_{i,r_i+1} = l_{i,r_i+1} \cdot (w_{i,1} - \hat{w}_{i,1}) \end{cases} \tag{13}$$

where $\hat{w}_{i,j}$ is the estimation of $w_{i,j}$, and $l_{i,j}$, $j = 1, \ldots, r_i + 1$, are gains of the observe and are chosen such that the roots of

$$s^{r_i+1} + l_{i,1} \cdot s^{r_i} + \cdots + l_{i,r_i} \cdot s + l_{i,r_i+1} = 0 \tag{14}$$

are in the left-half complex plane.

Using the estimation of perturbation $\hat{\Psi}_i = \hat{w}_{i,r_i+1}$ to compensate the real perturbation Ψ_i, the new control input vector $\boldsymbol{v} \in R^m$ can be obtained

$$\boldsymbol{u} = \boldsymbol{B}_0^{-1} \cdot \left\{ -\begin{bmatrix} \hat{\Psi}_1 \\ \vdots \\ \hat{\Psi}_m \end{bmatrix} + \boldsymbol{v} \right\} \tag{15}$$

3.1.3 Linear control method: Based on the new input–output relation, a linear controller can be introduced as

$$\begin{bmatrix} v_1 \\ \vdots \\ v_m \end{bmatrix} = \begin{bmatrix} y_{1\text{ref}}^{(r_1)} \\ \vdots \\ y_{m\text{ref}}^{(r_m)} \end{bmatrix} + \begin{bmatrix} k_{1,r_1} \cdot e_1^{(r_1-1)} + \cdots + k_{1,1} \cdot e_1 \\ \vdots \\ k_{m,r_m} \cdot e_m^{(r_m-1)} + \cdots + k_{m,1} \cdot e_m \end{bmatrix} \tag{16}$$

where $k_{p,q}$, $p = 1, \ldots, m$ and $q = 1, \ldots, r_p$ are gains of the linear controller, $y_{i\text{ref}}$ the desired output reference, and $e_i = y_{i\text{ref}} - y_i$ the tracking error. The error dynamics are given by

$$\begin{cases} e_1^{(r_1)} + k_{1,r_1} \cdot e_1^{(r_1-1)} + \cdots + k_{1,1} \cdot e_1 = 0 \\ \vdots \\ e_m^{(r_m)} + k_{m,r_m} \cdot e_m^{(r_m-1)} + \cdots + k_{m,1} \cdot e_m = 0 \end{cases} \tag{17}$$

With a well-designed $k_{p,q}$, desired system dynamics can be achieved.

3.2 Controller design

The presented NAC in Section 3.1 is then applied to design the controller of the EES-DVR in (4) and (5), and realise the performance comparison with the FLC. To save space, only the calculation results are given. The controller design using VC can refer to [16].

Firstly, the input–output linearisation of the DVR system is given by

$$\begin{bmatrix} \ddot{V}_{c\_d} \\ \ddot{V}_{c\_q} \end{bmatrix} = \begin{bmatrix} \omega \cdot \dot{V}_{c\_q} + \frac{1}{C} \cdot \omega \cdot I_{f\_q} - \frac{1}{C \cdot L} \cdot V_{c\_d} - \frac{1}{C} \cdot \dot{I}_{s\_d} \\ -\omega \cdot \dot{V}_{c\_d} - \frac{1}{C} \cdot \omega \cdot I_{f\_d} - \frac{1}{C \cdot L} \cdot V_{c\_q} - \frac{1}{C} \cdot \dot{I}_{s\_q} \end{bmatrix} + \begin{bmatrix} \frac{1}{C \cdot L} & 0 \\ 0 & \frac{1}{C \cdot L} \end{bmatrix} \cdot \begin{bmatrix} V_{f\_d} \\ V_{f\_q} \end{bmatrix} = \begin{bmatrix} F_1(\boldsymbol{x}) \\ F_2(\boldsymbol{x}) \end{bmatrix} + \begin{bmatrix} \boldsymbol{B}_1(\boldsymbol{x}) \\ \boldsymbol{B}_2(\boldsymbol{x}) \end{bmatrix} \cdot \begin{bmatrix} V_{f\_d} \\ V_{f\_q} \end{bmatrix} \tag{18}$$

3.2.1 Feedback linearising control: New system inputs are

$$\begin{bmatrix} V_{f\_d} \\ V_{f\_q} \end{bmatrix} = \begin{bmatrix} \boldsymbol{B}_1(\boldsymbol{x}) \\ \boldsymbol{B}_2(\boldsymbol{x}) \end{bmatrix}^{-1} \cdot \left\{ -\begin{bmatrix} F_1(\boldsymbol{x}) \\ F_2(\boldsymbol{x}) \end{bmatrix} + \begin{bmatrix} v_1 \\ v_2 \end{bmatrix} \right\} \tag{19}$$

The linear control method is expressed as

$$\begin{cases} v_1 = \ddot{V}_{c\_d\text{ref}} + k_{1,2} \cdot (\dot{V}_{c\_d\text{ref}} - \dot{V}_{c\_d}) + k_{1,1} \cdot (V_{c\_d\text{ref}} - V_{c\_d}) \\ v_2 = \ddot{V}_{c\_q\text{ref}} + k_{2,2} \cdot (\dot{V}_{c\_q\text{ref}} - \dot{V}_{c\_q}) + k_{2,1} \cdot (V_{c\_q\text{ref}} - V_{c\_q}) \end{cases} \tag{20}$$

3.2.2 Non-linear adaptive control: Perturbation terms are defined as

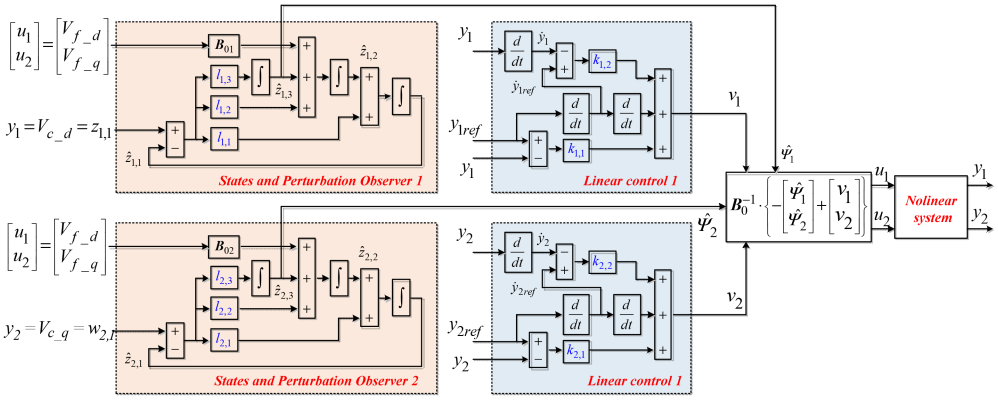

Fig. 3 *Block diagram of perturbation estimation-based NAC for the ESS-DVR*

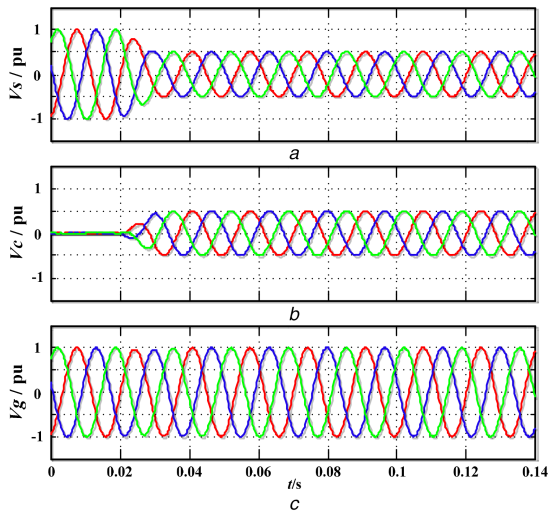

Fig. 4 *Performance of the NAC-based ESS-DVR in response to reduced (50%) grid voltage level*
(a) Grid voltage, ***(b)*** Compensation voltage, ***(c)*** Wind farm voltage

$$\begin{cases} \Psi_1 = F_1(\boldsymbol{x}) + [\boldsymbol{B}_1(\boldsymbol{x}) - \boldsymbol{B}_{01}(\boldsymbol{x})] \cdot \begin{bmatrix} V_{f\_d} \\ V_{f\_q} \end{bmatrix} \\ \Psi_2 = F_2(\boldsymbol{x}) + [\boldsymbol{B}_2(\boldsymbol{x}) - \boldsymbol{B}_{02}(\boldsymbol{x})] \cdot \begin{bmatrix} V_{f\_d} \\ V_{f\_q} \end{bmatrix} \end{cases} \tag{21}$$

High gain observers are given by

$$q_1: \begin{cases} \dot{\hat{w}}_{1,1} = \hat{w}_{1,2} + l_{1,1}(w_{1,1} - \hat{w}_{1,1}) \\ \dot{\hat{w}}_{1,2} = \hat{w}_{1,3} + l_{1,2}(w_{1,1} - \hat{w}_{1,1}) + \boldsymbol{B}_{01}(\boldsymbol{x}) \cdot \begin{bmatrix} V_{f\_d} & \\ & V_{f\_q} \end{bmatrix} \\ \dot{\hat{w}}_{1,3} = \dot{\hat{\Psi}}_1 = l_{1,3}(w_{1,1} - \hat{w}_{1,1}) \end{cases}$$
$$q_2: \begin{cases} \dot{\hat{w}}_{2,1} = \hat{w}_{2,2} + l_{2,1}(w_{2,1} - \hat{w}_{2,1}) \\ \dot{\hat{w}}_{2,2} = \hat{w}_{2,3} + l_{2,2}(w_{2,1} - \hat{w}_{2,1}) + \boldsymbol{B}_{02}(\boldsymbol{x}) \cdot \begin{bmatrix} V_{f\_d} & \\ & V_{f\_q} \end{bmatrix} \\ \dot{\hat{w}}_{2,3} = \dot{\hat{\Psi}}_2 = l_{2,3}(w_{2,1} - \hat{w}_{2,1}) \end{cases} \tag{22}$$

New system inputs are

$$\begin{bmatrix} V_{f\_d} \\ V_{f\_q} \end{bmatrix} = \begin{bmatrix} \boldsymbol{B}_{01}(\boldsymbol{x}) \\ \boldsymbol{B}_{02}(\boldsymbol{x}) \end{bmatrix}^{-1} \cdot \left\{ -\begin{bmatrix} \hat{\Psi}_1 \\ \hat{\Psi}_2 \end{bmatrix} + \begin{bmatrix} v_1 \\ v_2 \end{bmatrix} \right\} \tag{23}$$

The linear control method is obtained as

$$\begin{cases} v_1 = \ddot{V}_{c\_d\mathrm{ref}} + k_{1,2} \cdot (\dot{V}_{c\_d\mathrm{ref}} - \dot{V}_{c\_d}) + k_{1,1} \cdot (V_{c\_d\mathrm{ref}} - V_{c\_d}) \\ v_2 = \ddot{V}_{c\_q\mathrm{ref}} + k_{2,2} \cdot (\dot{V}_{c\_q\mathrm{ref}} - \dot{V}_{c\_q}) + k_{2,1} \cdot (V_{c\_q\mathrm{ref}} - V_{c\_q}) \end{cases} \tag{24}$$

To clearly illustrate the principle of the NAC, the block diagram of the NAC for ESS-DVR is given in Fig. 3. Note that the proposed NAC only requires the nominal values of system parameters and measurements of system outputs. Thus, it significantly reduces the controller complexity of the FLC by removing the requirement of a detailed system model and full-state feedback.

4 Simulation

Simulations are conducted based on the wind power system shown in Fig. 1 to test the LVRT capability enhancement by using the NAC-based ESS-DVR, comparing with the conventional VC and the accurate system model-based FLC. Parameters and control scheme of PMSG and DFIG in Fig. 1 come from [34].

Parameters of the NAC for subsystems 1 and 2 in Fig. 3 are designed based on the pole placement method: subsystem 1 observer 1: $l_{1,1} = 8$, $l_{1,2} = 0.3$, and $l_{1,3} = 7$; integral time constant: $T = 0.001$; controller 1: $k_{1,2} = 1 \times 10^5$ and $k_{1,1} = 2.4 \times 10^4$. Subsystem 2 observer 2: $l_{2,1} = 8$, $l_{2,2} = 0.3$, and $l_{2,3} = 7$; integral time constant: $T = 0.001$; controller 2: $k_{2,2} = 1 \times 10^5$, and $k_{2,1} = 2.4 \times 10^4$. The FLC uses the same parameters as that of the NAC. The parameters of the VC refer to [16], in which $k_P^v = 20$, $k_I^v = 10,000$, $k_P^c = 0.1$, and $k_I^c = 10$.

4.1 LVRT capability improvement

The LVRT capability enhancement of the wind farm by the NAC-based ESS-DVR is simulated under a reduced (50%) grid voltage level at 0.02 s at first. Simulation results are shown in Figs. 4–6.

From Fig. 4, the NAC-based ESS-DVR can quickly compensate the reduced grid voltage within 20–30 ms. As a result, the wind farm voltage V_g is only slightly affected by the voltage dip V_s in the power grid. Furthermore, different controllers, i.e. the VC and the FLC, are also designed and validated. Simulation results in Fig. 5 show that the NAC and the FLC have similar transient dynamics and they can greatly improve the LVRT capability compared to that of the VC for shorter settling time in wind farm voltage, the wind power, the DC-link voltage in PMSG-WTG, and the DC-link voltage in DFIG-WTG. The estimated perturbation terms in NAC are shown in Fig. 6. They comply with the real perturbations in FLC very well, which proves the effectiveness of the high gain observers.

In previous simulations, the GSC of the PMSG-WTG in wind farm is controlled by the conventional VC. Combined with our previous studies in [30] where the NAC is proposed for GSC controller design to enhance the LVRT capability of the PMSG-WTG, simulation results of both the ESS-DVR and the GSC of the PMSG-WTG controlled via NAC are given in Fig. 7. It shows that further but limited improvement on the LVRT capability of the wind farm. As a result, it is not necessary to apply NAC for all GSCs of PMSG-WTGs as the NAC-based ESS-DVR can solely compensate the grid voltage disturbance very well.

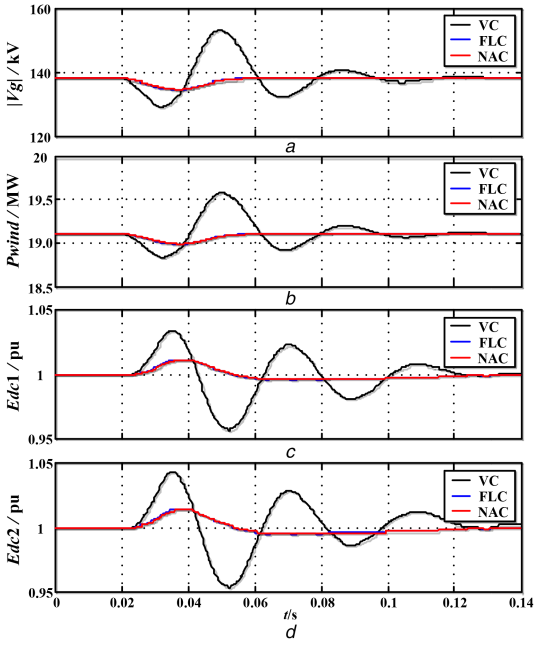

Fig. 5 *Performance of different controllers in response to reduced (50%) grid voltage level*

(a) Wind farm voltage, ***(b)*** Wind power, ***(c)*** DC-link voltage in PMSG-WTG, ***(d)*** DC-link voltage in DFIG-WTG

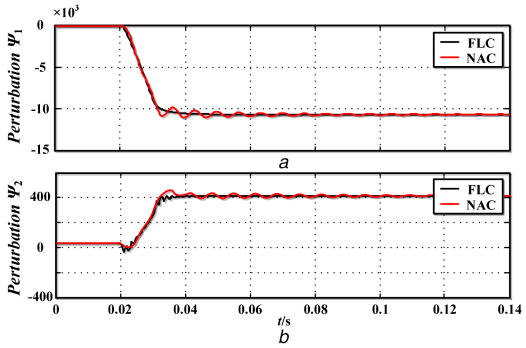

Fig. 6 *Estimation of the perturbation terms*

(a) Ψ_1, ***(b)*** Ψ_2

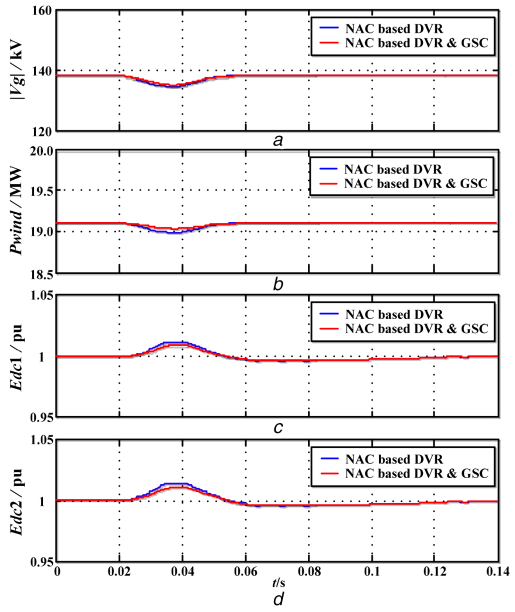

Fig. 7 *Coordination of the NAC-based ESS-DVR and the NAC-based GSC*

(a) Wind farm, ***(b)*** Wind power, ***(c)*** DC-link voltage in PMSG-WTG, ***(d)*** DC-link voltage in DFIG-WTG

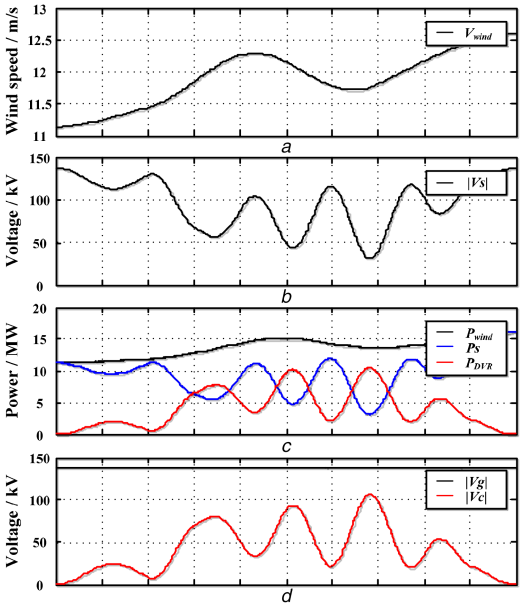

Fig. 8 *Control performance of the NAC-based ESS-DVR in complicated dynamic situation*

(a) Wind speed, ***(b)*** Grid voltage, ***(c)*** Power responses, ***(d)*** Wind farm voltage and compensation voltage

4.2 Dynamic performance under time-varying wind power and grid voltage

In the former analysis, the LVRT capability is investigated under steady-state condition, and a constant power output of the wind farm is assumed. Considering a complicated dynamic situation with fluctuating wind speed in Fig. 8*a* and varying grid voltage in Fig. 8*b*, satisfactory control performances can also be obtained by the proposed NAC-based ESS-DVR. For the reduced grid voltage, the wind power cannot be completely delivered to the grid (P_{wind}>P_s). The ESS-DVR thus absorbs and stores the transient surplus power P_{DVR} in Fig. 8*c* and injects compensation voltages V_{c} to achieve the constant wind farm voltage V_g in Fig. 8*d*.

4.3 Rating of DVR

From [15], the capacity of the ESS-DVR plays a key role in the LVRT capability enhancement. It depends mainly on the depth of the voltage fault that should be compensated. Therefore, simulation studies are conducted with different grid voltage levels to determine the appropriate capacity of the ESS-DVR. Under different gird voltage (from 0.0 to 0.8 p.u.), the relationship among the output power of wind farm P_{wind}, the power to the grid P_s, and the required power of the DVR P_{DVR} is shown in Fig. 9, which indicates that a larger ESS-DVR capacity is required for a deeper grid voltage dip level. If the capacity $S_{\text{ESS-DVR}}$ is insufficient, for example, a 10 MW ESS-DVR for dealing with a 40% V_{fault} which normally requires 12 MW ESS-DVR, the ESS-DVR only provides its maximum power and maintains reduced voltage level and increased current level, as shown in Fig. 10. In this case, wind farm should reduce the power output accordingly to avoid the overcurrent and protect the converters.

4.4 Robustness

Robustness of the NAC-based ESS-DVR has also been assessed under several typical simulation cases: grid voltage disturbances, wind power fluctuation, model uncertainties, and measurement noise, respectively.

4.4.1 Grid voltage disturbances: Responses of the DC-link voltage E_{dc1} in PMSG-WTG to different grid voltage levels (from 0.0 to 0.8 p.u.) are shown in Fig. 11. Responses of E_{dc2}, P_{wind}, and V_g are not presented due to the page limits.

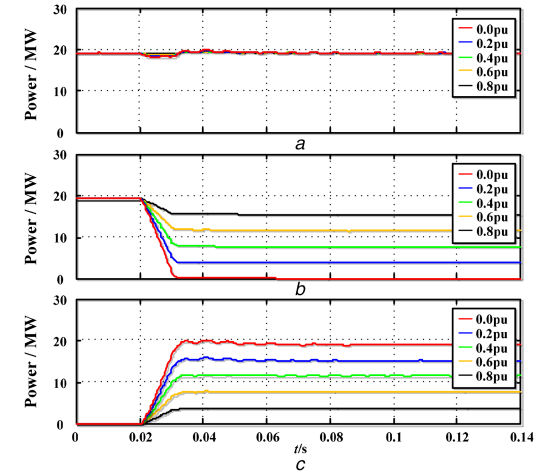

Fig. 9 *Power responses to different grid voltage levels*
(a) P_{wind}, ***(b)*** P_{S}, ***(c)*** P_{DVR}

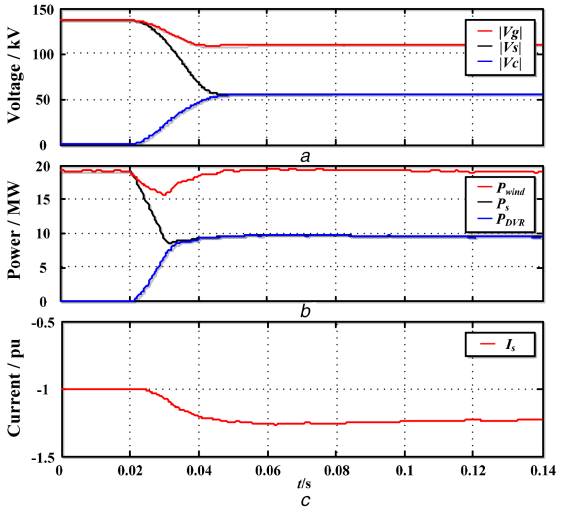

Fig. 10 *Performance of NAC-based ESS-DVR when the capacity is insufficient*
(a) Voltage, ***(b)*** Power responses, ***(c)*** Current

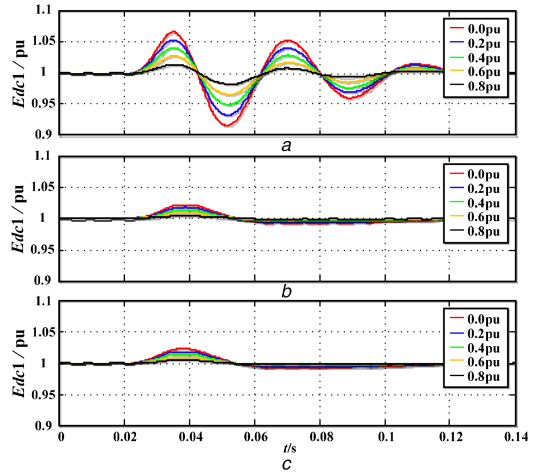

Fig. 11 *Response of DC-link voltage in PMSG-WTG to different grid voltage disturbances*
(a) VC, ***(b)*** FLC, ***(c)*** NAC

It shows that the dynamic of the DC-link voltage E_{dc1} by the VC has larger deviation and longer transient period than that of the FLC and the NAC which have similar dynamic responses. Furthermore, the FLC can behave a little better than the NAC because the NAC relies on the perturbation observer which has estimation error in practice. The FLC calculates the perturbation based on the assumption of accurate system model and measurements.

The peak value of E_{dc1} in Fig. 11 is listed in Table 1. The LVRT capability enhancement by the FLC and the NAC is about 66.7% compared to the VC.

4.4.2 Operating conditions: Considering different wind power, i.e. P_{wind} increasing from 120 to 200 MW, a reduced grid voltage level (50%) at 0.02 s is simulated. Fig. 12 shows that the influences of operating conditions on DC-link voltage in PMSG-WTG by the VC are about three times larger than that by the FLC and the NAC.

According to Table 1, it is concluded that VC is designed or tuned based on one operation point and may not be capable of providing consistent and optimal performance for different wind power, though a better tuning of the VC may result in a better performance. However, both the FLC and the NAC can achieve satisfactory performance under different grid voltage levels and wind power as the non-linear dynamics have been compensated.

4.4.3 Model uncertainties: The FLC is based on full-state feedback and accurate system model. The NAC employs the perturbation estimation and compensation and thus is theoretically immune to parameter uncertainties. Parameter uncertainties of the ESS-DVR are tested via several simulations performed for model mismatches of C and L in filters with ±20% uncertainties. All tests are under a reduced grid voltage level (50%).

As shown in Fig. 13, the peak DC-link voltage in PMSG-WTG controlled by the NAC is almost constant, while the FLC will result in small range of variation, especially for L model mismatch, i.e. 0.1%. This is because the proposed NAC estimates all uncertainties and does not need the accurate system model and thus has better robustness than the FLC which requires an accurate system model.

4.4.4 Measurement noise: The proposed NAC is an output feedback controller and only needs two measurements, the d-axis and q-axis components of the three-phase voltage V_{c}. However, the FLC requires all state variables and other measurements to calculate the system non-linearities. To test the robustness against the measurement noise, the white noise of +2% and −2% of voltage is injected into $V_{\text{c\_}d}$ and $V_{\text{c\_}q}$, respectively.

As shown in Figs. 14 and 15, the performance of the NAC is almost not affected by the noise in the measurement of compensation voltage, but the performance of the FLC has been degraded greatly, especially when ±2% white noise is injected into $V_{\text{c\_}d}$.

5 Conclusion

A perturbation compensation-based NAC is presented in this paper to control the ESS-DVR in improving the LVRT capability of wind farms. This control is independent of accurate system model and full-state feedbacks. In addition, it can adaptively estimate and compensate uncertainties and external disturbances including different grid voltage dips and intermittent wind power inputs. The ESS-DVR is controlled to quickly compensate the grid voltage dips to support the PCC's voltage and store the blocked wind power for potential wind power fluctuation suppression. The LVRT capability enhancement by using the NAC is tested and compared with the VC and the FLC-based ESS-DVR. The main conclusions are given below.

Both the NAC-based and the FLC-based ESS-DVR can greatly improve the LVRT capability of wind farms comparing with the VC. Moreover, the NAC-based ESS-DVR shows a satisfactory improvement of the dynamic performance under time-varying wind power and grid voltage disturbances.

The relationship between the capacity of ESS-DVR and the voltage fault level has been assessed via simulation studies. A larger ESS-DVR capacity is required for a deeper grid voltage dip

Table 1 Peak value of DC-link voltage in PMSG-WTG

Control method	Grid voltage level, p.u.				
	0.8 p.u.	0.6 p.u.	0.4 p.u.	0.2 p.u.	0.0 p.u.
VC	1.014	1.027	1.041	1.054	1.066
FLC	1.004	1.009	1.013	1.018	1.022
NAC	1.005	1.009	1.014	1.018	1.023

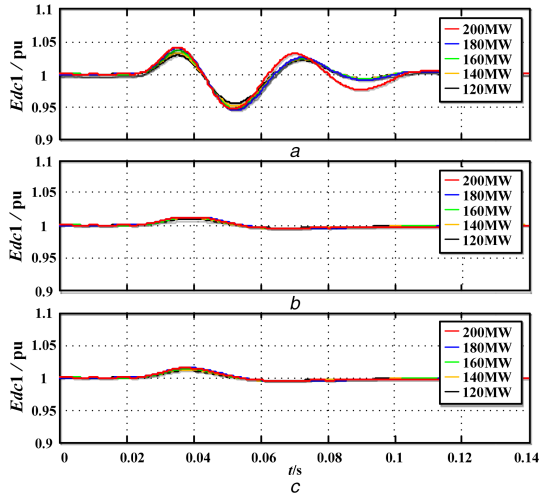

Fig. 12 *Response of DC-link voltage in PMSG-WTG to different wind power*
(a) VC, ***(b)*** FLC, ***(c)*** NAC

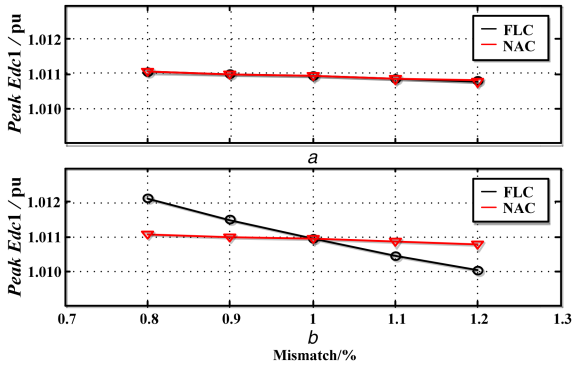

Fig. 13 *Peak DC-link voltage in PMSG-WTG to a reduced (50%) grid voltage level for model uncertainties in the range of ±20% (one parameter changes and others keep constant)*
(a) C model mismatch, ***(b)*** L model mismatch

level. If the DVR capacity is insufficient, a reduced control performance will be expected.

Under varying grid voltage disturbances and operating conditions, both the NAC and the FLC show better robustness than the VC because the non-linear dynamics are well compensated. Further, the NAC has a relatively simpler controller and could have much better robustness than the FLC, especially in the case of model uncertainties and measurement noise.

6 Acknowledgments

This work was supported by the National Key Research and Development Program of China (2017YFB0902000), and the Natural Science Foundation of China under grants (51607092).

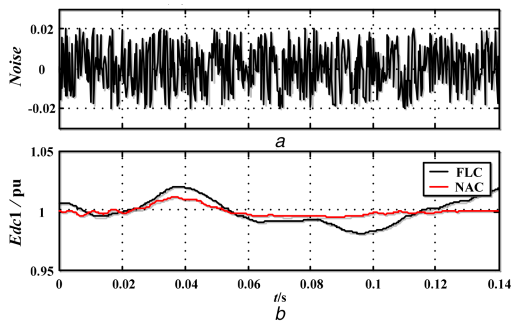

Fig. 14 *Response of DC-link voltage in PMSG-WTG to a reduced (50%) grid voltage level with ±2% white noise injected into V_{c_d}*
(a) Measurement noise, ***(b)*** DC-link voltage in PMSG-WTG

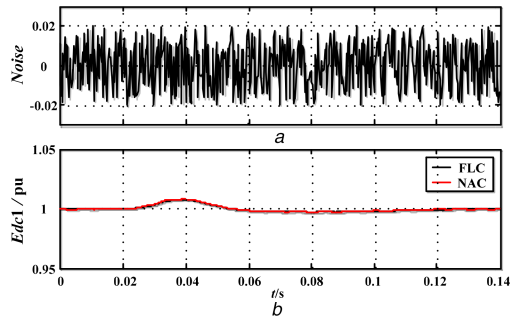

Fig. 15 *Response of DC-link voltage in PMSG-WTG to a reduced (50%) grid voltage level with ±2% white noise injected into V_{c_q}*
(a) Measurement noise, ***(b)*** DC-link voltage in PMSG-WTG

7 References

[1] Ramirez, D., Martinez, S., Platero, C.A., *et al.*: 'Low-voltage ride-through capability for wind generators based on dynamic voltage restorers', *IEEE Trans. Energy Convers.*, 2011, **26**, (1), pp. 195–203

[2] Howlader, M., Senjyu, T.: 'A comprehensive review of low voltage ride through capability strategies for the wind energy conversion systems', *Renew. Sust. Energy Rev.*, 2016, **56**, pp. 643–658

[3] Nasiri, M., Milimonfared, J., Fathi, S.H.: 'A review of low-voltage ride-through enhancement methods for permanent magnet synchronous generator based wind turbines', *Renew. Sust. Energy Rev.*, 2015, **47**, pp. 399–415

[4] Justo, J.J., Mwasilu, F., Jung, J.W.: 'Doubly-fed induction generator based wind turbines: a comprehensive review of fault ride-through strategies', *Renew. Sust. Energy Rev.*, 2015, **47**, pp. 447–467

[5] Thet, A.K., Saitoh, H.: 'Pitch control for improving the low-voltage ride-through of wind farm'. 2009 Transmission & Distribution Conf. & Exposition: Asia and Pacific, Seoul, 26–30 October 2009, pp. 1–4

[6] Alepuz, S., Calle, A., Monge, S.B., *et al.*: 'Use of stored energy in PMSG rotor inertia for low-voltage ride-through in back-to-back NPC converter-based wind power systems', *IEEE Trans. Ind. Electron.*, 2013, **60**, (5), pp. 1787–1796

[7] Liang, J.Q., Qiao, W., Harley, R.G.: 'Feed-forward transient current control for low-voltage ride-through enhancement of DFIG wind turbines', *IEEE Trans. Energy Convers.*, 2010, **25**, (3), pp. 836–843

[8] Hossain, M.J., Saha, T.K., Mithulananthan, N., *et al.*: 'Control strategies for augmenting LVRT capability of DFIGS in interconnected power systems', *IEEE Trans. Ind. Electron.*, 2013, **60**, (6), pp. 2510–2522

[9] Nguyen, T.H., Lee, D.C.: 'Ride-through technique for PMSG wind turbines using energy storage systems', *J. Power Electron.*, 2010, **10**, (6), pp. 733–738

[10] Pannell, G., Atkinson, D.J., Zahawi, B.: 'Minimum-threshold crowbar for a fault-ride-through grid-code-compliant DFIG wind turbine', *IEEE Trans. Energy Convers.*, 2010, **25**, (3), pp. 750–759

[11] Nguyen, T.H., Lee, D.C.: 'Advanced fault ride-through technique for pmsg wind turbine systems using line-side converter as STATCOM', *IEEE Trans. Ind. Electron.*, 2013, **60**, (7), pp. 2842–2850

[12] Yang, J., Fletcher, J.E., Reilly, J.O.: 'A series-dynamic-resistor-based converter protection scheme for doubly-fed induction generator during

various fault conditions', *IEEE Trans. Energy Convers.*, 2010, **25**, (2), pp. 422–432

[13] Qiao, W., Venayagamoorthy, G.K., Harley, R.G.: 'Real-time implementation of a statcom on a wind farm equipped with doubly fed induction genrators', *IEEE Trans. Ind. Appl.*, 2009, **45**, (1), pp. 98–107

[14] Molinas, M., Suul, J.A., Undeland, T.: 'Low voltage ride through of wind farms with cage generators: STATCOM versus SVC', *IEEE Trans. Power Electron.*, 2008, **23**, (3), pp. 1104–1117

[15] Wessels, C., Gebhardt, F., Fuchs, F.W.: 'Fault ride-through of a DFIG wind turbine using a dynamic voltage restorer during symmetrical and asymmetrical grid faults', *IEEE Trans. Power Electron.*, 2011, **26**, (3), pp. 807–815

[16] Ibrahim, A.O., Hguyen, T.H., Lee, D.C*., et al.*: 'A fault ride-through technique of DFIG wind turbine systems using dynamic voltage restorers', *IEEE Trans. Energy Convers.*, 2011, **26**, (3), pp. 871–882

[17] Hussein, A.A., Hasan Ali, M.: 'Comparison among series compensators for transient stability enhancement of doubly fed induction generator based variable speed wind turbines', *IET Renew. Power Gener.*, 2016, **10**, (1), pp. 116–126

[18] Alaraifi, S., Moawwad, A., Moursi, M.S.E*., et al.*: 'Voltage booster schemes for fault ride-through enhancement of variable speed wind turbines', *IEEE Trans. Sustain. Energy*, 2013, **4**, (4), pp. 1071–1081

[19] Leon, A.E., Farias, M.F., Battaiotto, P.E*., et al.*: 'Control strategy of a DVR to improve stability in wind farms using squirrel-cage induction generators', *IEEE Trans. Power Syst.*, 2011, **26**, (3), pp. 1609–1617

[20] Nielsen, J.G., Newman, M., Nielsen, H*., et al.*: 'Control and testing of a dynamic voltage restorer (DVR) at medium voltage level', *IEEE Trans. Power Electron.*, 2004, **19**, (3), pp. 806–813

[21] Ajaei, F.B., Afsharnia, S., Kahrobaeian, A*., et al.*: 'A fast and effective control scheme for the dynamic voltage restorer', *IEEE Trans. Power Deliv.*, 2011, **26**, (4), pp. 2398–2406

[22] Jurado, F., Valverde, M.: 'Fuzzy logic control of a dynamic voltage restorer'. IEEE Int. Symp. on Industrial Electronics, Ajacco, France, May 2004, pp. 1047–1052

[23] Hawatt, E.E., Hamad, M.S., Ahmed, K.H*., et al.*: 'Low voltage ride-through capability enhancement of a DFIG wind turbine using a dynamic voltage restorer with adaptive fuzzy PI controller'. Int. Conf. on Renewable Energy Research and Applications, Madrid, October 2013, pp. 1234–1239

[24] Li, Y.W., Blaabjerg, F., Vilathgamuwa, D.M*., et al.*: 'Design and comparison of high performance stationary-frame controllers for dvr implementation', *IEEE Trans. Power Electron.*, 2007, **22**, (2), pp. 602–612

[25] Jurado, F., Hidalgo, F.P.: 'Neural network control for dynamic voltage restorer'. IEEE 2002 28th Annual Conf. of the Industrial Electronics Society, Sevilla, November 2002, pp. 615–620

[26] Cheng, P.T., Chen, J.M., Ni, C.L.: 'Design of a state-feedback controller for series voltage-sag compensators', *IEEE Trans. Ind. Appl.*, 2009, **45**, (1), pp. 260–267

[27] Jeong, S.Y., Nguyen, T.H., Lee, D.C*., et al.*: 'Nonlinear control of three-phase four wire dynamic voltage restorers for distribution system'. 2014 Int. Power Electronics Conf., May 2014, Hiroshima, pp. 2406–2412

[28] Chen, S., Joos, G., Lopes, L*., et al.*: 'A nonlinear control method of dynamic voltage restorers'. 2002 IEEE 33rd Annual Power Electronics Specialists Conf., Cairns, Queensland, 2002, pp. 88–93

[29] Sarhangzadeh, M., Hosseini, S.H., Sharifian, M.B.B*., et al.*: 'Dynamic analysis of DVR implementation based on nonlinear control by IOFL'. 2011 24th Canadian Conf. on Electrical and Computer Engineering, Niagara Falls, May 2011, pp. 264–269

[30] Chen, J., Jiang, L., Yao, W*., et al.*: 'Perturbation estimation based nonlinear adaptive control of a full-rated converter wind turbine for fault ride-through capability enhancement', *IEEE Trans. Power Syst.*, 2014, **29**, (6), pp. 2733–2743

[31] Liu, Y., Wu, Q.H., Zhou, X.X*., et al.*: 'Perturbation observer based multiloop control for the DFIG-WT in multimachine power system', *IEEE Trans. Power Syst.*, 2014, **29**, (6), pp. 2905–2915

[32] Jiang, L., Wu, Q.H., Wen, J.Y.: 'Decentralized nonlinear adaptive control for multi-machine power systems via high-gain perturbation observer', *IEEE Trans. Circuit Syst. I Regul. Papers*, 2004, **51**, (10), pp. 2052–2059

[33] Wu, Q.H., Jiang, L., Wen, J.Y.: 'Decentralized adaptive control of interconnected non-linear systems using high gain observer', *Int. J. Control*, 2004, **77**, (8), pp. 703–712

[34] Clark, K., Miller, N.W., Sanchez-Gasca, J.J.: 'Modeling of GE wind turbine-generators for grid studies', Technical Report, GE Energy, September 2009